WEP Warwick Evans Publishing

International Journal of Computer Science and Information Technology

ISSN: 3005-9682 (Print), ISSN: 3005-7140 (Online) | Volume 7, Number 2, Year 2025
DOI: https://doi.org/10.62051/ijcsit.v7n2.06
Journal homepage: https://wepub.org/index.php/IJCSIT/index

Numerical Simulation of the Mixing Process for Natural Gas–Hydrogen Blends in a T-Junction Pipe

Shihua Ren *

College of Petroleum Engineering, Xi'an Shiyou University, Xi'an, China
*Corresponding Author: Shihua Ren

ABSTRACT

Against the backdrop of energy decarbonization, utilizing existing natural gas pipelines for hydrogen blending represents a critical pathway for large-scale hydrogen transportation. This study employs numerical simulations using ANSYS Fluent, incorporating the species transport model and the Realizable k-ε turbulence model, to investigate the mixing process of hydrogen and methane within a T-junction pipeline. The effects of hydrogen blending ratio, flow velocity, injection position, and pipeline pressure on the mixing effectiveness are analyzed. The Coefficient of Variation (COV) is used to evaluate the mixing uniformity length. The results indicate that significant hydrogen stratification occurs initially in the pipeline, with diffusion and gradual homogenization occurring along the flow length. Within the hydrogen blending range of 5% to 20%, the difference in mixing length is limited. An increase in flow velocity extends the mixing distance due to reduced residence time. Injection from the bottom of the pipeline significantly shortens the mixing length (shortest at 9.1 m). Increasing the pressure to 0.6 MPa enhances mixing, but further pressure increases yield limited additional benefit.

KEYWORDS

Hydrogen-blended natural gas; T-junction; Numerical simulation; Mixing uniformity; Coefficient of variation (COV); ANSYS Fluent

1. INTRODUCTION

Against the backdrop of the accelerating global energy transition, hydrogen energy has emerged as a core area in the competition for dominance in energy technologies among major global economies, owing to its clean, efficient, and versatile application prospects [1]. Developed countries such as Japan, Germany, and the United States have established strategic frameworks encompassing the entire hydrogen industry chain, including production, storage, transportation, and application. China, as the world's largest hydrogen producer, has initially formed five regional industrial clusters, guided by policies like the "Medium and Long-Term Plan for the Development of the Hydrogen Energy Industry." The global hydrogen sector is currently undergoing a critical shift from "gray hydrogen" to "green hydrogen." Although China is experiencing rapid growth in the scale of renewable energy-based hydrogen production, the transportation of hydrogen remains a significant challenge hindering the development of the hydrogen industry chain [2, 3].

In recent years, blending hydrogen into natural gas pipelines for transportation has become a key research focus among scholars. Given that natural gas pipeline technology is already well-established, numerous natural gas pipelines have been planned and constructed worldwide. Compared to building dedicated pure hydrogen pipelines, transporting hydrogen-blended natural gas (HBNG) offers a lower-cost conversion by leveraging existing natural gas pipeline infrastructure. This approach

represents one of the most viable methods for achieving large-scale, long-distance, safe, and efficient hydrogen transportation [4, 5].

However, the significant density difference between hydrogen and natural gas can easily lead to flow stratification during pipeline transportation. Due to buoyancy effects, hydrogen tends to accumulate in the upper section of the pipeline, creating a longitudinal concentration gradient. This stratification phenomenon becomes particularly pronounced under low flow velocities or during pipeline shutdowns [6].

Although blending hydrogen into natural gas pipelines offers numerous advantages, the introduction of hydrogen presents risks of material failure mechanisms such as hydrogen embrittlement and hydrogen-induced cracking. HAESELDONCKX et al. [7] found that natural gas pipelines face an increased risk of hydrogen-induced failure after hydrogen blending, especially when microcracks are present due to fatigue damage, significantly raising the probability of such failures. ZHOU Hui et al. [8], by developing a segmented throttling coefficient prediction model (with an error $\leq 1.68\%$ for high-concentration blends), revealed the impact of different hydrogen blending ratios on the throttling characteristics of natural gas pipelines and proposed a safety threshold of $\leq 30\%$ hydrogen blending ratio. YIN Xiaona et al. [9] utilized ANSYS Fluent software for simulation calculations to analyze the effect of hydrogen addition on the measurement accuracy of ultrasonic flow meters in natural gas pipelines. By investigating the mixing behavior of hydrogen and natural gas, they found that injecting hydrogen from the bottom of the pipeline can reduce the required mixing length.

2. MODEL ESTABLISHMENT

2.1. Blending Pipeline Model

This study established a T-junction pipeline model using Design Modeler and conducted a numerical simulation of the hydrogen-natural gas mixing process within the T-junction using the ANSYS Fluent software platform. The research aims to systematically investigate the influence of key parameters, including mainstream flow velocity, blending ratio, hydrogen injection angle, and pipeline operating pressure, on the mixing effectiveness.

Regarding model construction, the Species Transport model was employed to accurately describe the multi-component mixing process. This model solves the mass conservation equations for each component, enabling it to precisely capture the concentration gradient distribution and diffusion behavior between hydrogen and natural gas. It is particularly suitable for analyzing mixing problems with significant concentration differences. The Realizable k-ε model was selected as the turbulence model. Compared to the standard k-ε model, it offers superior predictive capabilities under conditions of strong shear flow and rotational flow. Its improved formula for calculating turbulent viscosity allows for more accurate simulation of the complex vortex structures generated during the mixing process, thereby yielding more reliable predictions of mixing performance.

The setting of the mixed gas physical properties fully considered the interactions between components: Density was calculated using the volume-weighted mixing law. This method computes the mixture density by weighting the volume fractions, accurately reflecting the volumetric contribution of each component during mixing. Specific heat capacity was determined using the mixing law, which is suitable for thermodynamic calculations of ideal gas mixtures. Thermal conductivity and viscosity were both calculated using the mass-weighted mixing law. This approach computes transport properties by weighting mass fractions, enabling a more precise description of inter-component energy and momentum transfer processes. The mass diffusion coefficient was calculated based on kinetic theory. This method, rooted in molecular collision theory, allows for accurate prediction of the mutual diffusion behavior between different components.

Boundary Conditions Setup: The inlet was defined as a velocity inlet, allowing precise control of the mass flow rate at each intake. The outlet was set as a pressure outlet with the no-backflow option enabled to ensure computational stability. All wall surfaces were assigned the no-slip boundary condition, consistent with the physical characteristics of real-world flow.

The calculation was initialized using the standard initialization method, with initial field variables appropriately configured to facilitate rapid convergence of the computational process. The entire solution procedure employed second-order discretization schemes and adhered to strict convergence criteria (energy residual < 10^{-6}, residuals for other variables < 10^{-3}) to ensure the reliability of the numerical simulation results.

2.2. Mathematical Model Formulation

Continuity Equation:

$$\frac{\partial \rho}{\partial t} + \nabla \cdot (\rho \vec{v}) = S_m \tag{1}$$

Where ρ is the fluid density, and S_m is a user-defined source term.

Momentum Conservation Equation:

$$\frac{\partial}{\partial t}(\rho \vec{v}) + \nabla \cdot (\rho \vec{v} \vec{v}) = -\nabla p + \nabla \cdot (\bar{\bar{\tau}}) + \rho \vec{g} + \vec{F} \tag{2}$$

$$\bar{\bar{\tau}} = \mu \left[(\nabla \vec{v} + \nabla \vec{v}^T) - \frac{2}{3} \nabla \cdot \vec{v} I \right] \tag{3}$$

Where p is the static pressure; $\bar{\bar{\tau}}$ is the stress tensor; $\rho \vec{g}$ represents gravitational body forces; $\vec{F}$ encompasses external body forces and other model-dependent source terms; μ denotes molecular viscosity; and I is the unit tensor.

Energy Conservation Equation:

$$\frac{\partial}{\partial t}(\rho E) + \nabla \cdot (\bar{v}(\rho E + p)) = -\nabla \cdot (\sum_j h_j J_j) + S_h \tag{4}$$

As an enhancement to the $RNG\ k-\varepsilon$ and other turbulence models, the Re*alizable* k-ε was introduced. The term "Re*alizable*" signifies that the model satisfies certain mathematical constraints consistent with the physics of turbulence. In the Realizable Re*alizable* k-ε, the transport equations are defined as:

$$\frac{\partial}{\partial t}(\rho k) + \frac{\partial}{\partial x_j}(\rho k u_j) = \frac{\partial}{\partial x_j}\left[(\mu + \frac{\mu_i}{\sigma_k}) \frac{\partial k}{\partial x_j} \right] + G_k + G_b - \rho \varepsilon - Y_M + S_k \tag{5}$$

$$\frac{\partial}{\partial t}(p\varepsilon) + \frac{\partial}{\partial x_j}(p\varepsilon u_j) = \frac{\partial}{\partial x_j}[(\mu + \frac{\mu_i}{\sigma_\varepsilon}) \frac{\partial k}{\partial x_j}] + \rho C_1 S_\varepsilon - \rho C_2 \frac{\varepsilon^2}{k + \sqrt{\nu \varepsilon}} C_{1\varepsilon} \frac{\delta}{k} C_{3\varepsilon} G_b + S_\varepsilon \tag{6}$$

Where:

G_k represents the generation of turbulent kinetic energy due to mean velocity gradients; G_b denotes the generation of turbulent kinetic energy due to buoyancy; Y_M represents the contribution of fluctuating dilatation in compressible turbulence to the overall dissipation rate; C_2 and $C_{1\varepsilon}$ are constants; σ_k and σ_ε are the turbulent Prandtl numbers for k and ε, respectively; S_k and S_ε are user-defined source terms.

Where:

$$C_1 = \max\left[0.43, \frac{\eta}{\eta+5}\right],\ \eta = S\frac{k}{g},\ S = \sqrt{2S_{ij}S_{ij}},\ C_{1\varepsilon} = 1.44,\ C_2 = 1.9\ \sigma_k = 1.0\ \sigma_\varepsilon = 1.2$$

$$\mu_t = \rho C_\mu \frac{k^2}{\varepsilon} \tag{7}$$

$$C_\mu = \frac{1}{A_0 + A_s\frac{kU^*}{\varepsilon}} \tag{8}$$

Where Ω is the mean rate-of-rotation tensor observed in a moving reference frame with angular velocity ω; A_0 and A_s are constants.

$$U^* = \sqrt{S_{ij}S_{ij} + \tilde{\Omega}_{ij}\tilde{\Omega}_{ij}},\ \tilde{\Omega}_{ij} = \Omega_{ij} - 2\varepsilon_{ijk}\omega_k,\ \Omega_{ij} = \bar{\Omega}_{ij} - \varepsilon_{ijk}\omega_k,\ A_0 = 4.04,\ A_S = \sqrt{6}\cos\phi,$$
$$\phi = \frac{1}{3}\cos^{-1}(\sqrt{6}W),\ W = \frac{S_{ij}S_{jk}S_{ki}}{S^3},\ \tilde{S} = \sqrt{S_{ij}S_{ij}},\ S_{ij} = \frac{1}{2}\left(\frac{\partial u_j}{\partial x_i} + \frac{\partial u_i}{\partial x_j}\right)$$

Species Transport Model:

$$\frac{\partial}{\partial t}(\rho Y_i) + \nabla\cdot(\rho\vec{v}Y_i) = -\nabla\cdot\vec{J}_i + R_i + S_i \tag{9}$$

Where R_i is the net rate of production of species i by chemical reactions, and S_i is the rate of generation due to the addition of dispersed phase and user-defined source terms.

Mass Diffusion in Turbulent Flow:

$$\vec{J}_i = -(\rho D_{i,m} + \frac{\mu_t}{Sc_t})\nabla Y_i - D_{T,i}\frac{\nabla T}{T} \tag{10}$$

Where $D_{i,m}$ is the mass diffusion coefficient for species iin the mixture, $D_{T,i}$ is the thermal diffusion coefficient, Sc_t is the turbulent Schmidt number, $Sc_t = 0.7$

Calculation of Diffusion Coefficient:

$$D_{AB} = \frac{0.0101T^{1.75}(1/M_A + 1/M_B)^{1/2}}{p\left[(\sum_v)_A^{1/3} + (\sum_v)_B^{1/3}\right]^2}[81-83] \tag{11}$$

Where D_{AB} is the molecular diffusion coefficient of gas component A in B, in m^2/s; T is the temperature of the gas mixture, in K; M_A and M_B are the molar masses of gas components A and B, respectively, in kg/mol; p is the total pressure of the gas mixture, in Pa; $(\sum_v)_A$ and $(\sum_v)_B$ are the diffusion volumes of gas components A and B, respectively, in cm^3/mol.

2.3. Model Description and Mesh Generation

This study established a T-junction pipeline model using Design Modeler, performed mesh generation via Workbench Meshing, and conducted simulations and post-processing of hydrogen-natural gas blending using Fluent. The mixing process in the T-junction involves complex physical phenomena such as fluid interfaces and turbulent diffusion, which are highly sensitive to mesh resolution. Excessively coarse meshes may lead to distorted calculations of diffusion coefficients and inaccurate predictions of hydrogen concentration distributions, while overly refined meshes significantly increase computational costs. Thus, a balance between computational accuracy and efficiency is essential.

To determine the optimal mesh size, a grid independence verification was conducted. As shown in Table 1, when the mesh size was progressively refined from 10 mm to 5 mm, the corresponding cell count increased from 2,341,406 to 9,715,611, and the calculated pressure drops across the pipeline were 50.38 Pa, 51.19 Pa, 52.53 Pa, 53.67 Pa, 54.28 Pa, and 54.01 Pa, respectively. Notably, when the mesh size was refined to 7 mm, further reduction to 5 mm resulted in a pressure drop variation of less than 1.2%, while computational resource consumption increased exponentially. Based on this analysis, a mesh size of 7 mm (corresponding to 4,948,140 cells) was selected. This approach ensures a pressure drop calculation error of less than 1.5% while significantly improving computational efficiency.

Table 1. Grid Independence Verification

Mesh Size (mm)	Mesh Size (mm)	Mesh Size (mm)
10	2341406	50.38
9	2920215	51.19
8	3739520	52.53
7	4948140	53.67
6	6823654	54.28
5	9715611	54.01

An unstructured mesh was adopted with boundary layer refinement (as shown in Fig. 1). This mesh strategy effectively captures the flow characteristics near the wall region while resolving concentration gradients in the multi-component mixing process through local refinement of the mixing zone. The optimized mesh system provides a reliable numerical foundation for subsequent fluid analyses, such as blending ratio and concentration field distribution.

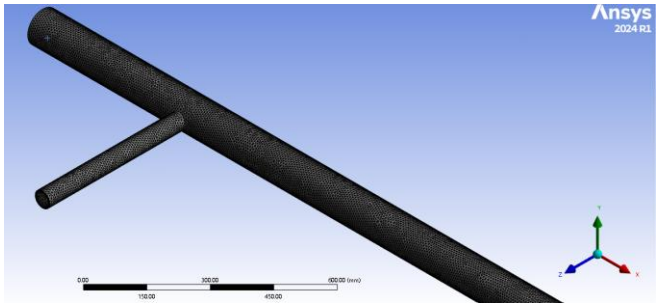

Figure 1. Mesh Generation Diagram

3. RESULTS AND DISCUSSION

3.1. Analysis of Gas Flow Characteristics

Under the conditions of a methane inlet velocity of 4 m/s, a hydrogen blending ratio of 20%, and hydrogen injected from the top, the simulated velocity distribution contour on the x-zcross-section obtained via Fluent is shown in Fig. 2.

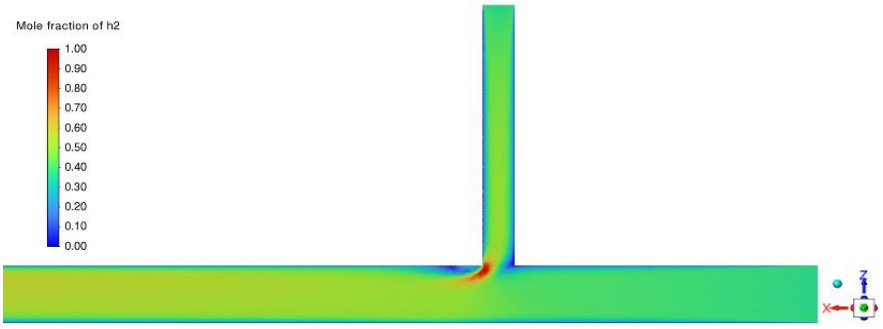

Figure 2. Velocity nephogram at the pipeline inlet section

As shown in Fig. 2, when hydrogen is injected from the upper pipeline at 4 m/s, its velocity increases rapidly upon entering the main pipe due to the impact and entrainment by methane flowing from the right at 4 m/s. A localized high-velocity region forms near the junction, with a maximum velocity of approximately 10.77 m/s, significantly higher than the individual inlet velocities of hydrogen and methane. Subsequently, the velocity of the mixture gradually decreases and stabilizes, though a relatively low-velocity blue region persists near the upper hydrogen inlet, indicating the influence of hydrogen flow on the mainstream methane flow. This low-velocity region gradually dissipates at a distance of 50 mm from the center of the junction. The central region of the pipeline exhibits a slight increase in velocity while maintaining relatively uniform motion, whereas the near-wall region shows lower velocities approaching zero.

Regarding the mixing characteristics of hydrogen and methane in the pipeline, the concentration contour is shown below: A significant stratification phenomenon is observed near the mixing point, with a transverse extension of approximately half the pipe diameter. The initial mixing stage corresponds to the velocity contour, where the injected hydrogen is impacted and entrained by methane.

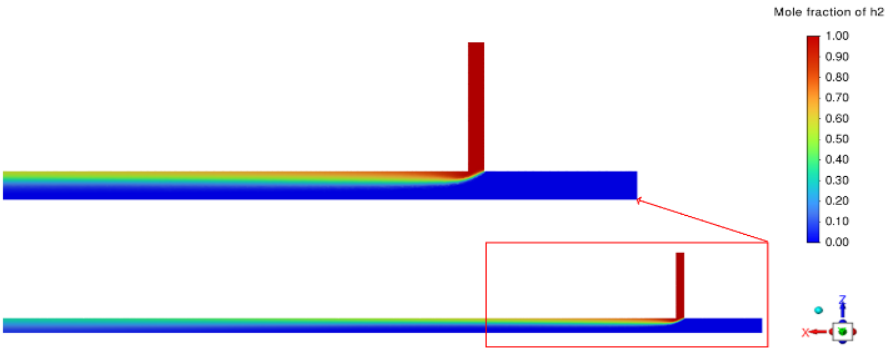

Figure 3. Hydrogen-methane molar fraction distribution contour on the x-z plane

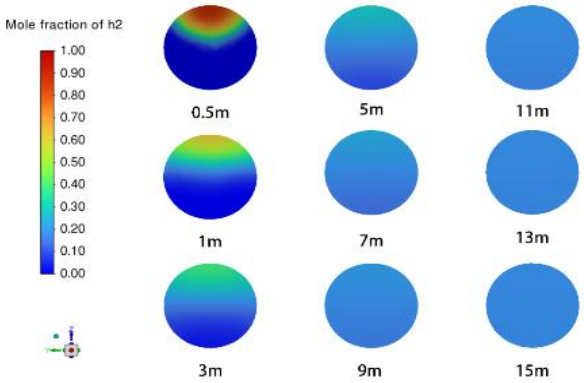

Figure 4. Hydrogen-methane molar fraction distribution contour on the y-z pla

Figs. 3 and 4 present the hydrogen-methane molar fraction distribution contours at different cross-sections, clearly illustrating the mixing process of hydrogen within the pipeline. At a distance of 0.5 m from the injection point, the contour exhibits a distinct red-blue alternating pattern, indicating significant concentration gradients at this cross-section. This suggests that hydrogen has not yet fully diffused and remains concentrated in the upper region of the pipeline. As the mixing length increases, the contour transitions to similar shades of blue, demonstrating reduced heterogeneity in hydrogen concentration and gradual homogenization of the mixture.

Quantitative evaluation of mixing effectiveness employs a multi-parameter statistical analysis approach, focusing on three core indicators: Analysis of Variance (ANOVA), Relative Standard Deviation (RSD), and Coefficient of Variation (COV). In the study of hydrogen-methane blending systems, the Coefficient of Variation (COV) is selected as the evaluation metric for mixing uniformity.

The specific definition and implementation procedure are as follows:

After quantitatively injecting hydrogen into the inlet section of the blending pipeline, a gridded sampling model is established at the target detection cross-section—the selected cross-section is divided into N subunits, and the measured hydrogen concentration value C_{hi} for each subunit i is recorded.

$$COV = \frac{\sigma}{c} = \frac{\sqrt{\frac{1}{N}\sum (c_i - \overline{c})^2}}{\frac{1}{N}\sum c_i} \times 100\% \tag{12}$$

Where c_i: hydrogen concentration value in the i -th subunit; $\overline{c}$: average hydrogen concentration value in the i-th region of the cross-section; σ: standard deviation of hydrogen concentration values; c: average hydrogen concentration value across the entire cross-section.

From a fluid dynamics perspective, the uniformity of the mixing process can be quantitatively evaluated using statistical indicators. The Coefficient of Variation (COV), as a measure of relative standard deviation, effectively reflects the dispersion degree of the concentration field. Based on engineering practice data, a COV value below 5% is generally considered to indicate basic uniformity, while a value exceeding 15% suggests significant local enrichment or stratification phenomena. Due to differences in molecular motion characteristics, mixing behaviors vary distinctly across different material systems. Given the high diffusion rates of gaseous media, this study sets a stricter COV threshold of 2%.

In the experimental design, a spatially discrete sampling-based concentration monitoring method was adopted. Specifically, multiple monitoring cross-sections were arranged along the mixing pipeline: the first monitoring surface was positioned 0.5 m downstream from the mixing point, followed by additional sections at intervals of 1 m (i.e., at 1 m, 2 m, 3 m, etc.). By collecting hydrogen

concentration data from sampling points at each cross-section and calculating the corresponding COV values, the variation in mixing effectiveness along the pipeline length could be clearly observed. This approach enabled quantitative evaluation of the pipeline length required to achieve mixing uniformity, thereby accurately characterizing the blending performance.

3.2. Effect of Hydrogen Blending Ratio on Mixing Performance

This study systematically evaluated the influence of hydrogen blending ratio on mixing performance using a controlled variable method. The baseline conditions were set with a methane flow velocity of 4 m/s, and four hydrogen blending ratio gradients were tested: 5%, 10%, 15%, and 20%.

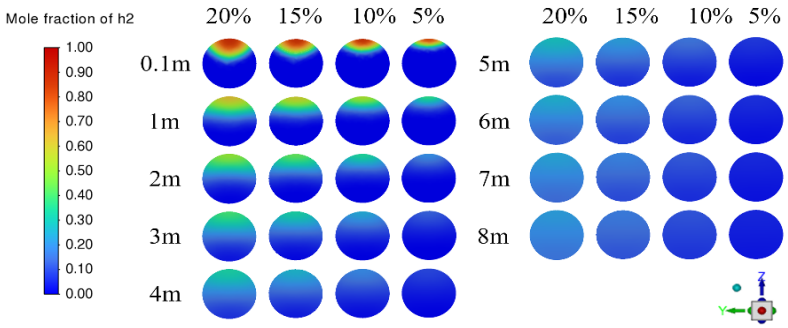

Figure 5. Hydrogen Molar Fraction Distribution Contours at Different Blending Ratios

Table 2. Grid Independence Verification

Methane Inlet Velocity (m/s)	Methane Inlet Velocity (m/s)	Methane Inlet Velocity (m/s)	Methane Inlet Velocity (m/s)
4	4	20	13.1
4	2.82	15	13.4
4	1.78	10	13.6
4	0.84	5	13.7

Table 2 presents the pipeline lengths required to achieve mixing uniformity under different hydrogen blending ratios, while Fig. 5 shows the corresponding contours of hydrogen molar concentration distribution. Data analysis indicates that as the hydrogen blending ratio decreases from 20% to 5%, the mixing length exhibits a monotonic increasing trend (from 13.1 m to 13.7 m). This pattern can be attributed to two primary mechanisms: The reduction in hydrogen jet momentum leads to diminished turbulent mixing intensity. Specifically, when the blending ratio decreases from 20% to 5%, the hydrogen jet momentum is reduced by 79%; The lowered concentration gradient weakens the driving force for molecular diffusion. The initial concentration gradient at the 5% blending condition is only 25% of that observed at the 20% blending condition.

3.3. Influence of Gas Flow Velocity on Mixing Performance

Numerical simulations were conducted to systematically investigate the effects of inlet flow velocity on mixing performance while maintaining a constant hydrogen blending ratio of 20%. The methane inlet velocity was varied from 4 m/s to 9 m/s in 1 m/s increments, with corresponding proportional adjustments to hydrogen injection rates to preserve the specified blending ratio. The Coefficient of Variation (COV) was calculated to determine the pipeline length required to achieve mixing uniformity (COV $\leq$ 2%). The resulting mixing lengths are presented in Table 3.

Table 3. Mixing Length under Varied Inlet Velocities (20% H_2 Blending Ratio)

Methane Inlet Velocity (m/s)	Methane Inlet Velocity (m/s)	Methane Inlet Velocity (m/s)	Methane Inlet Velocity (m/s)
4	4	13.1	4
5	5	13.7	5
6	6	14.2	6
7	7	14.7	7
8	8	14.4	8
9	9	14.6	9

As can be seen from the data in Table 3, as the inlet flow velocity increases from 4 m/s to 7 m/s, the mixing uniformity length exhibits a monotonically increasing trend, rising from 13.1 m to 14.7 m. However, when the flow velocity further increases to 8 m/s and 9 m/s, the mixing uniformity length shows slight fluctuations, measuring 14.4 m and 14.6 m, respectively. This phenomenon can be attributed to the increase in the Reynolds number (Re) within the pipe as the flow velocity increases, leading to enhanced turbulence intensity. Theoretically, higher turbulence intensity should promote mixing efficiency, allowing the gas to achieve uniformity more rapidly. However, in this study, the mixing uniformity length increases with higher flow velocities, indicating that turbulence intensity is not the sole determining factor. The increase in flow velocity reduces the residence time of the gas within the pipe. When the flow velocity increases from 4 m/s to 7 m/s, although turbulence intensity is enhanced, the reduced mixing time may be insufficient to fully leverage the advantages of turbulent mixing. Consequently, a longer pipe length is required to achieve mixing uniformity.

3.4. The Impact of Hydrogen Blending Location on Mixing Effectiveness

Under the condition of maintaining all other parameters constant, simulations were conducted by varying the hydrogen injection location for analysis. The coefficient of variation (CV) at each interface was calculated, and the mixing effectiveness was evaluated based to the distance required to achieve homogeneous mixing

This simulation was performed with a hydrogen blending ratio of 20% and a flow velocity of both hydrogen and natural gas set at 4 m/s. Sequential numerical simulations were carried out, followed by computation of the coefficient of variation. The resulting mixing lengths required to attain uniformity are presented in the table 4:

Table 4. Mixing Length under Varied Inlet Velocities

Injection Angle	Injection Orientation	Length Required for Homogeneous Mixing (m)
90°	Top	13.1
90°	Center	12.8
90°	Bottom	9.1
45°	Top	13.6
45°	Center	13.2
45°	Bottom	10.3
135°	Top	12
135°	Center	11.3
135°	Bottom	9.6

Simulations with different hydrogen injection locations were conducted under a 20% hydrogen blending ratio and an inlet velocity of 4 m/s. The results indicate that, at the same injection angle, bottom injection achieves better mixing performance compared to lateral or top injection. This

phenomenon can be attributed to the density difference between hydrogen and natural gas: hydrogen, being less dense than methane, tends to rise upward when injected from the bottom, while the denser methane above sinks downward due to gravity. This counter-flow movement induced by buoyancy effects enhances convective mixing and thereby improves overall blending efficiency.

3.5. The Influence of Pressure on Mixing Effectiveness

Under the condition of constant other parameters, the impact of pressure variations on mixing performance was investigated by adjusting the pipeline pressure. The simulation results are as follows:

Table 5. Mixing Length under Varied Inlet Pressure

Pressure (kPa)	Pressure (kPa)
400	13.1
500	13
600	12.8
700	12.8

Analysis of the simulation results indicates that as the pipeline pressure increases from 400 kPa to 700 kPa, the mixing length decreases from 13.1 m to 12.8 m and subsequently stabilizes. This suggests that within the 400–600 kPa range, elevated pressure enhances mixing by increasing gas density and turbulence intensity: higher pressure reduces the mean free path of gas molecules, thereby augmenting intermolecular collision frequency. Simultaneously, the increase in Reynolds number intensifies vortex motion, accelerating the transverse diffusion of hydrogen. Beyond 600 kPa, the flow field structure stabilizes, and turbulence intensity reaches a saturated state. Further pressure increases yield diminishing returns in mixing improvement.

4. CONCLUSIONS

(1) When hydrogen is injected into the main natural gas pipeline, it is impacted by the methane mainstream, forming a localized high-velocity region with a peak velocity of 10.77 m/s, significantly higher than the inlet velocity. A distinct low-velocity zone emerges near the hydrogen injection point, which extends 50 mm along the flow direction before gradually dissipating. The central region of the pipeline maintains a uniform velocity of approximately 4 m/s, while the near-wall region approaches zero velocity due to wall friction. Concentration distribution reveals transverse stratification during the initial mixing stage, spanning approximately half of the pipe diameter. The correspondence between velocity and concentration fields indicates that the impact of the methane mainstream is the primary mechanism enhancing mixing.

(2) Hydrogen blending ratio, flow velocity, injection location, and system pressure significantly influence the mixing performance of natural gas-hydrogen blends. Variations in the hydrogen blending ratio within the 5%–20% range result in a minimal difference of only 0.6 m in the mixing length, indicating a relatively limited impact. Increased flow velocity prolongs the mixing distance due to reduced residence time. The injection location exhibits the most substantial influence: bottom injection leverages buoyancy effects most effectively, reducing the mixing length to a minimum of 9.1 m. Elevating system pressure to 0.6 MPa enhances mixing by intensifying turbulence, but further pressure increases yield diminishing returns as the effect saturates. These findings provide critical theoretical guidance for optimizing concentration monitoring point placement, pipeline structural design, and adaptive blending systems in natural gas-hydrogen blending processes.

CONFLICTS OF INTEREST

The authors declare that no potential conflict of interest exists with respect to the research, authorship, and/or publication of this article.

ACKNOWLEDGEMENTS

The successful completion of this research would not have been possible without the support and guidance from numerous individuals and organizations. First and foremost, I wish to express my deepest gratitude to my research supervisor, Professor Qing Quan of Xi'an Shiyou University, for his invaluable guidance, insightful suggestions, and unwavering encouragement throughout this study. I am also deeply thankful to my colleagues at the Multiphase Flow Laboratory for their constructive discussions and technical support during the simulation and data analysis phases. Special thanks go to the anonymous reviewers and editors for their valuable comments, which significantly improved the quality of this manuscript. Lastly, I extend my heartfelt appreciation to my family and friends for their unconditional support, understanding, and patience throughout my graduate studies.

REFERENCES

[1] Li Zheng, Zhang Rui, Sun Hexu, et al. Review on Key Technologies of Hydrogen Generation, Storage and Transportation Based on Multi-Energy Complementary Renewable Energy [J]. Transactions of China Electrotechnical Society, 2021, 36(3): 446-462.

[2] Ban, J.; Yan, X.; Song, B.; Deng, S.; Wu, H.; Tang, Y.; Yin, W. Research Progress and Prospects on Hydrogen Damage in Welds of Hydrogen-Blended Natural Gas Pipelines. Processes 2023, 11, 3180. https://doi.org/10.3390/pr11113180

[3] Medium and long term planning for the development of hydrogen energy industry (2021-2035) [R]. Beijing: National Development and Reform Commission of the People's Republic of China , 2022:2-3.

[4] ZHANG Jiajun, GUO Liping. Latest progress in hydrogen pipeline transportation technology [J]. Chemical Industry and Engineering Progress, 2024, 43(12): 6692-6699.

[5] GAO Yue, ZHU Hongjun, TANG Tang, et al. Research status and analysis of hydrogen-blended natural gas transportation in natural gas pipelines [J]. Low-carbon Chemistry and Chemical Engineering, 2024, 49(03):118-128. DOI: 10.12434/j.issn.2097-2547.20230260.

[6] Li, T.; Xiao, J.; Zhang, H.; Cheng, J.; Li, K.; Wang, Y.; Lin, Y. Numerical Simulation Study of Gas Stratification in Hydrogen-Enriched Natural Gas Pipelines. Energies 2025, 18, 3181.

[7] HAESELDONCKX D, D'HAESELEER W. The use of the natural-gas pipeline infrastructure for hydrogen transport in a changing market structure [J]. International Journal of Hydrogen Energy, 2007, 32(10/11):1381-1386.

[8] Su Y, Li J, Yu B, et al. Study of Hydrogen Stratification Phenomena in Hydrogen-Blended Natural Gas Pipelines [J]. Renewable Energy, 2025: 123603.

[9] Shouhu J I, Chen S U N, Yongwei A N, et al. Investigation on Adaptability of Ultrasonic Flowmeter for Hydrogen Blended to Natural Gas Pipeline Structure [J]. Mechanics in Engineering, 2023, 45(2): 333-344.